Fracture assessment of V-notched specimens with end holes made of tungsten-copper functionally graded material under mode I loading

H.Salavati[a] H.Mohammadi[b] A.Yusefi[c] F.Berto[d]

https://doi.org/10.1016/j.tafmec.2017.06.013Get rights and content

Abstract

The present research is the first to assess fracture of V-notches with end holes (VO-notches) made of tungsten-copper functionally graded material (W-Cu FGM) under mode I both experimentally and theoretically. W-Cu FGM specimens were fabricated by powder metallurgy technique. A number of fracture tests were carried out on VO-notched W-Cu FGM specimens under mode I for various notch tip radii, notch depths, and notch opening angles.

The averaged strain energy density over a well-defined control volume was employed to predict the fracture loads. A numerical approach was used to determine the outer boundary of the control volume. Besides, the effect of notch geometry (notch tip radius, notch depth, and notch opening angle) on fracture load was elaborated. This study demonstrates that SED works well on VO-notched FGM specimens under mode I loading.

Keywords

Functionally graded materials
Tungsten
Copper
V-notches with end hole
Mode I
Strain energy density

1. Introduction

Evaluation of brittle fracture in notched components is a serious subject which has involved many researchers. Notches are stress concentrator parts which mainly cause strength weakening in structures, however, strengthening behavior of notched components has recently been reported in some cases [1]. Prediction of static and fatigue failure of structures is a challenging topic which has attracted a great

interest [2], [3], [4]. Several researchers have proposed some fracture criteria to assess the critical fracture load of notched components. One of the most prominent criteria is the volume based strain energy (SED) criterion which reminds the Sih's criterion [5] combining the local mode I [6] and elementary volume concepts. The averaged SED criterion which has been applied first to pointed V notches [7] and later extended to blunt notches [8] states that brittle fracture takes place if the averaged value of the SED over a well-defined control volume reaches its critical value. A lot of research has been conducted dealing with U-[9], [10], [11], [12], [13] and V-[14], [15], [16], [17], [18] notches considering SED criterion. In recent years, several assessments have been made on key-hole notches and V-notches with end holes (VO-notches) which appear in the structures due to applying a conventional repairing method on cracked U- and V-notches [19], [20], [21]. The mentioned repairing technique is to drill a circular hole on the notch tip with a hole radius equal to the crack length. The closed form equations which were obtained by Zappalorto and Lazzarin [22] for stress distribution can be considered the first effort which was directly made on VO-notches. Based on fictitious notch rounding (FNR) concept, a number of assessments were made regarding mode I [23], [24], mode II [25], mode III [26] and mixed mode I-II [27], [28]. Some other criteria such as SED [19], [29], [30], PS [31], [32], MS [31], [32], [33], [34] and MTS [33], [34]have been employed to investigate the fracture of VO-notches under different loading modes. Berto et al. [29] assessed the brittle fracture of VO-notches using specimens made of isostatic polycrystalline graphite under compressive mode (mode I). By means of the averaged SED criterion they obtained the fracture loads and compared with experimentally measured ones and a good agreement was observed. In parallel, Torabi et al. [30] studied the brittle failure of VO-notched Brazilian disk specimens made of PMMA under tension mode by means of the averaged SED criterion. Taking advantage of their experimental tests they showed that the averaged SED criterion is applicable for VO-notches under tensilemode as well. Recently, Torabi et al. [19] investigated pure mode II fracture of VO-notches both experimentally and theoretically. They provided a set of experimental tests on PMMA Brazilian disk specimens weakened by VO-notches. It was demonstrated that the local strain energy density criterion is suitable for VO-notches also under pure mode II. Although various works have been done on VO-notches, a small number of them are allocated to the fracture of functionally graded materials [35].

Functionally Graded Materials (FGM) are characterized by a gradual change in material properties over volume. FGMs are anisotropic composite materials where a material gradient has been deliberately introduced over two different materials. The gradient can

for example be in composition and/or in microstructure. By applying this concept, materials like ceramics and metals can be brought together with a gradual change from one material to another which results in some specific properties. Different types of FGMs have been fabricated in recent years. Tungsten-copper functionally graded materials (W-Cu FGM) are a type of FGMs which are known as widely-used materials due to their applications as ultra-high voltage electric contact materials and heat-sink materials [36]. Large differences in melting point between these two metals make it difficult to produce W-Cu FGM. Different fabrication techniques namely spark plasma sintering [37], microwave sintering [38], laser sintering [39], one-step resistance sintering [40], etc. have been employed to produce W-Cu FGMs. Various works on the mechanical and thermal behavior of W-Cu FGMs have been done [41], [42], [43], [44], [45], [46]. Prediction of fracture of W-Cu FGM specimens weakened by notches is another important topic to assess.

Regarding brittle or quasi-brittle static fracture of FGMs, some papers have been published on U-[47], [48], [49], [50], [51] and V-[52], [53], [54], [55] notches. Barati et al. [47] studied the effect of notch depth on J-integral and fracture load of U-notched Al-SiC specimens under mode I loading condition. The fracture loads were predicted using three criteria namely point stress, mean stress, and the averaged strain energy density and compared with experimentally measured ones. In addition, a comparison between homogeneous and functionally graded Al-SiC was made. It was shown that functionally graded Al-SiC was more convenient than homogeneous Al-SiC against fracture.

In this research, the fracture of W-Cu FGM specimens has been studied. A new set of experimental results have been presented on VO-notches under mode I loading. The averaged strain energy density criterion has been used to predict the critical fracture loads. Besides, the effect of notch geometries (e.g. notch tip radius, notch opening angle, and notch depth) on fracture load has been investigated.

2. Experiments

2.1. Material and mechanical properties

In this paper, W-Cu FGM specimens having six layers have been fabricated by powder metallurgy method. There is a gradual change from a tungsten-based alloy (WBA) with the chemical composition of W-Ni-Mn-Cu respectively as 90–4–3.33–2.67 wt.% to pure copper. High purity (>99% purity) fine-grained (particle size of 7.5–30 μm) elemental powders were used as received without any modification. The six-layered W-Cu FGM specimens were produced with the content of WBA as 100%, 80%, 60%, 40%, 20%,

and 0% (vol.%) in each layer, respectively. Table 1 shows the chemical composition and theoretical density of each layer.

Table 1. Chemical composition and theoretical density of layers.

Layer no.	WBA (Vol.%)	Cu (Vol.%)	Chemical composition of layers (Wt.%)				Theoretical density of layers (gr/cm^3)
			W	Ni	Mn	Cu	
1	100	0	90	4	3.33	2.67	17.176
2	80	20	71.61	3.18	2.65	22.56	15.678
3	60	40	53.41	2.37	1.98	42.23	14.108
4	40	60	35.42	1.57	1.31	61.7	12.472
5	20	80	17.61	0.78	0.65	80.95	10.758
6	0	100	0	0	0	100	8.96

The composition of WBA (layer 1) was made mixing tungsten, copper, nickel, and manganese powders in a high-energy ball milling system. In order to obtain the composition of layers 2–5, WBA and copper powders were mixed in a ball milling system with respect to the content of each item (Table 1). The powders of layers 1–6 were stacked layer-by-layer into a D2 steel die with the diameter of 25 mm and height of 50 mm. Thicknesses of the layers were considered to be 1, 0.5, 0.5, 0.5, 0.5, and 1 mm for each layer, respectively. So the amount of powder of each layer was determined using the theoretical densities. The stacked powders were pressed at room temperature under a pressure of 500 MPa. The green compact was ejected from the die. The sintering process was performed in a vacuum furnace at a heating rate of 10 °C/min. Sintering temperature and pressure were set to be 1050 °C and 10^{-5} mbar, respectively. Specimens were sintered at that temperature for 3 h and were cooled in the furnace. Both sides of the sintered specimens were ground and the final thickness of 4 mm was reached by grinding. Then notched specimens were drawn by a high precision electro discharge wire cut machine. Fig. 1 depicts the fabrication procedure schematically.

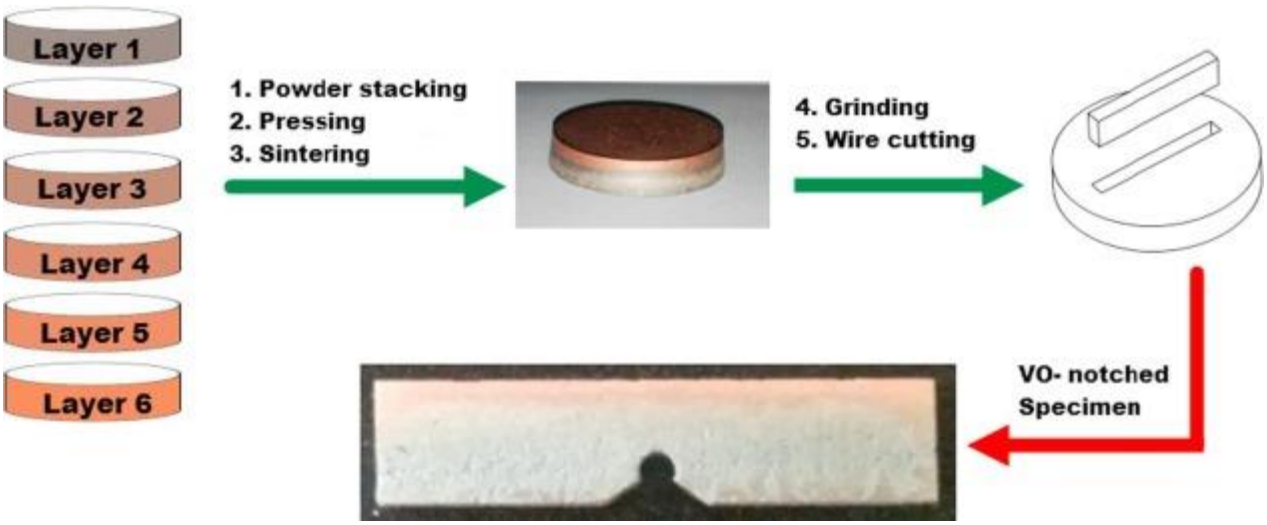

1. Download high-res image (98KB)
2. Download full-size image

Fig. 1. Fabrication procedure of W-Cu FGM Specimens.

In order to present some functions for mechanical properties, the specimens were assumed to consist 3 regions, WBA region, copper region, and the graded region which connects the WBA region to copper region (Fig. 2). In other words, 4 innermost layers (layers 2–5) were considered as the graded region. The thicknesses of regions were determined using metallography techniques. The averaged thickness of WBA region, the graded region, and copper region were obtained to be 0.95 mm, 2.3 mm, and 0.75 mm, respectively. The power law function was employed to describe mechanical properties of the graded region.

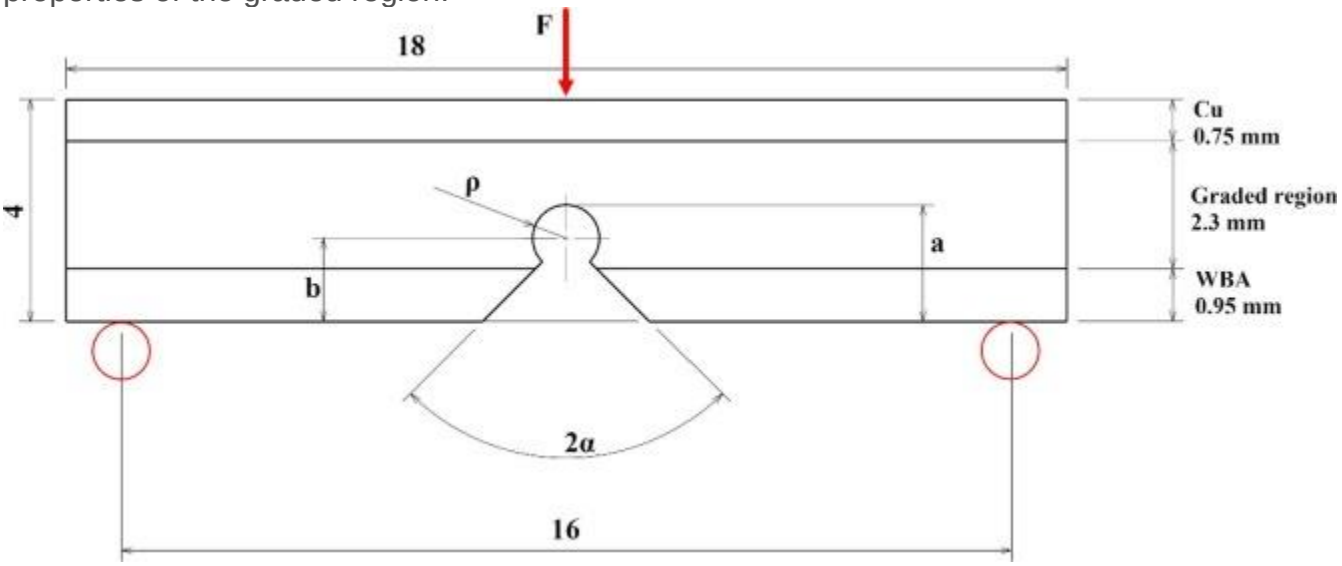

1. Download high-res image (57KB)
2. Download full-size image

Fig. 2. SENB specimen geometries (dimension are in millimeters), thickness = 2 mm.

As is suggested in [51] the power law function was employed to describe mechanical properties of the graded region and the elasticity modulus, Poisson's ratio, ultimate tensile stress, and fracture toughness (K_{Ic}) can be obtained using the following functions:

(1)E(Z)=[ECu-EWBA]2Z+h2hn+EWBA

(2)v(Z)=[vCu-vWBA]2Z+h2hn+vWBA

(3)σut(Z)=[σutCu-σutWBA]2Z+h2hn1+σutWBA

(4)KIc(Z)=[KIcCu-KIcWBA]2Z+h2hn2+KIcWBA

where E is the elasticity modulus, v is the Poisson's ratio, σ_{ut} is the ultimate tensile stress, K_{Ic} is the fracture toughness, n, n_1, n_2 are the power law exponents, Z is the thickness coordinate of the graded region ($-h/2 < Z < h/2$), and h is the thickness of the graded region (h = 2.3 mm). Indexes Cu and WBA shows the properties of copper and WBA. The boundary condition properties and power law exponents of Eqs. (1), (2), (3), (4) are presented in Table 2:

Table 2. Mechanical properties of boundary layers.

Boundary regions	Elasticity modulus E(GPa)	Poisson's ratio v	Ultimate tensile stress σ_{ut} (MPa)	Fracture toughness K_{Ic} (MPa m$^{0.5}$)	n	n_1	n_2
Cu	112.7	0.34	188.9	88.5	0.9646	1.312	2.78
WBA	289.5	0.29	447.3	4.52			

2.2. Specimens and experimental tests

Three-point bending tests were performed on single edge VO-notched (SENB) specimens. Thickness, width, and length of the specimens were set to be equal to 2 mm, 4 mm, and 18 mm, respectively. Dimensions were in agreement with ASTM E1820. The span lengthbetween two supports was set to be 16 mm. The load was applied on the notch bisector line in order to obtain mode I loading condition. Fig. 2 illustrates loading condition and geometryof the specimens. VO-notches were drawn from WBA side. Three notch tip radii (ρ) of 0.3, 0.4, 0.6 mm and three notch opening angles (2α) of 60, 90, and 120° were considered in experimental tests. In all specimens, the depth of the center of curvature (b) was equal to 1 mm. In total, nine different geometrical configurations were prepared (Fig. 3.).

1. Download high-res image (119KB)
2. Download full-size image

Fig. 3. Different SENB VO-notched specimens.

For each geometrical configuration, three specimens were tested providing 27 new experimental data for mode I loading in W-Cu FGM. The experiments were performed by a ZWICK 1494 testing device under displacement control with a constant displacement rate of 0.05 mm/min. Fig. 4 shows a SENB VO-notched specimen under three-point bending test. The fracture loads of each test and also the mean value F_{EXP} are summarized in Table 3.

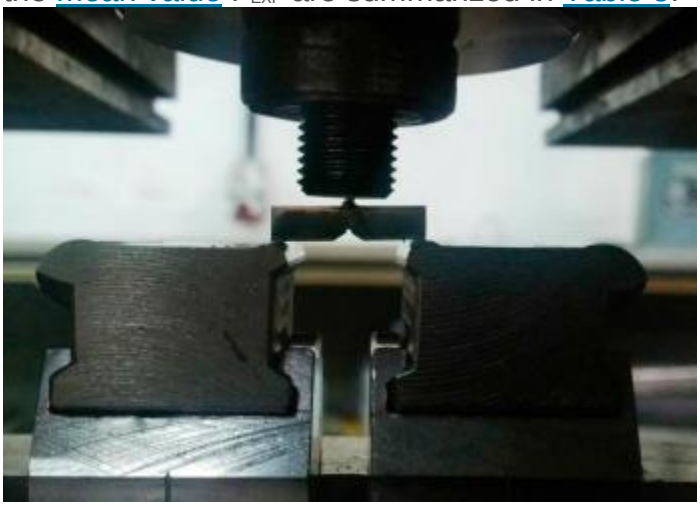

1. Download high-res image (112KB)
2. Download full-size image

Fig. 4. A SENB VO-notched W-Cu FGM specimen under mode I loading.

Table 3. Experimental values of fracture load (F_1, F_2, and F_3) and mean value F_{EXP}.

ρ (mm)	b (mm)	2α (°)	F_1 (N)	F_2 (N)	F_3 (N)	F_{EXP} (N)
0.3	1	60	103.5	99.2	85.5	96.1
0.4	1	60	119.9	96.8	98.5	105.1

ρ (mm)	b (mm)	2α (°)	F_1 (N)	F_2 (N)	F_3 (N)	F_{EXP} (N)
0.6	1	60	118.7	120.6	124.9	121.4
0.3	1	90	115.1	95.3	90.3	100.2
0.4	1	90	105.4	115.4	101.1	107.3
0.6	1	90	120.1	131.0	106.4	119.2
0.3	1	120	87.6	82.0	95.6	88.4
0.4	1	120	105.4	113.2	103.3	107.3
0.6	1	120	104.1	108.9	135.7	116.2

3. Averaged SED criterion over a well-defined control volume

The averaged SED criterion states that brittle fracture occurs when the averaged value of the SED over a well-defined control volume is equal to a critical value W_c[17]. W_c is a material-dependent value which is independent of notch geometry. For brittle materials, $W_c$can be evaluated as follow [17]:

(5)Wc=σut22E

For a VO-notch under mode I loading, the control volume assumes the crescent shape which is centered in relation to the notch bisector line as shown in Fig. 5. R_c is the critical length which is measured along the notch bisector line.

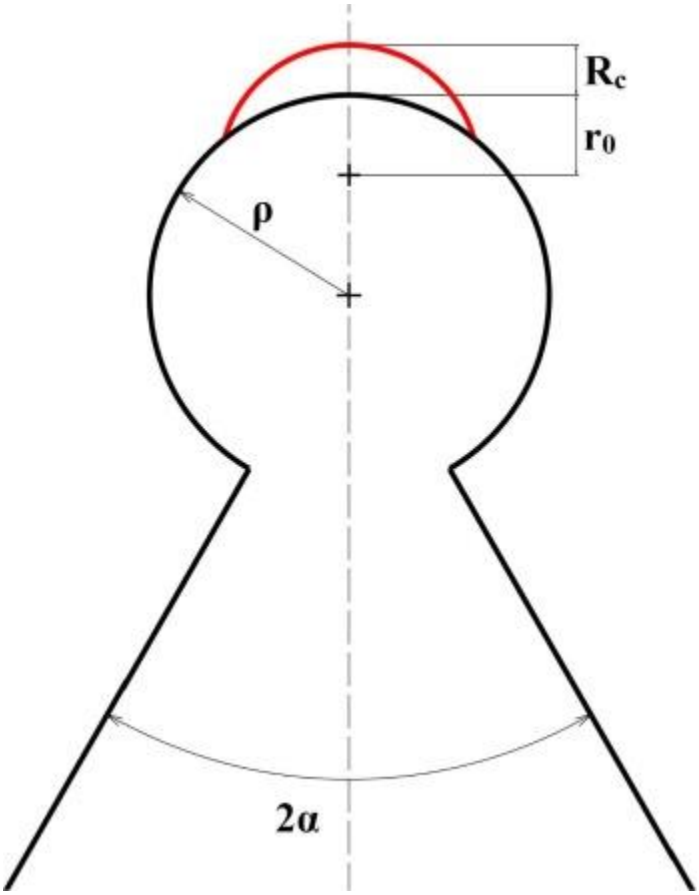

1. Download high-res image (58KB)
2. Download full-size image

Fig. 5. Control volume for a VO-notched homogeneous specimen under mode I.

The critical length (R_c) can be evaluated as follow under plane strain conditions [56], [57]:

(6)Rc=(1+v)(5-8v)4πKIcσut2

where K_{Ic} is the fracture toughness, σ_{ut} is the ultimate tensile stress and v is the Poisson's ratio. The outer radius of the control volume is equal to $R_c + r_0$ as shown in Fig. 5. The value of r_0 can be determined as follow [8]:

(7)r0=q-1qρq=2π-2απ

In homogeneous materials, R_c is constant all over the specimen. In comparison, in nonhomogeneous materials, R_c varies point by point due to a gradual change in material properties. In a nonhomogeneous medium with a smooth unidirectional variation in mechanical properties in the x-direction (along the notch depth), the outer boundary of the control volume is assumed oval shape as shown schematically in Fig 6.

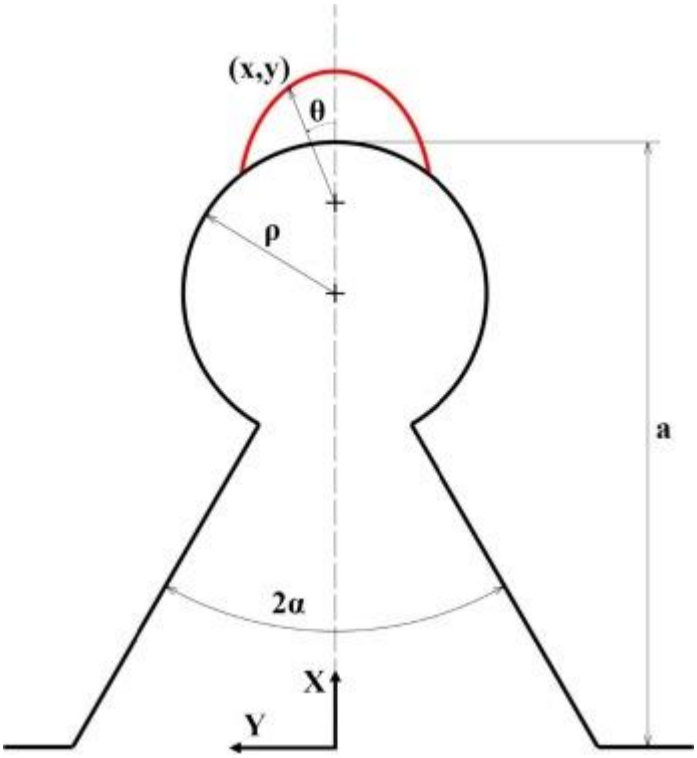

1. Download high-res image (55KB)
2. Download full-size image

Fig. 6. Control volume for a VO-notched FGM specimen under mode I.

For a VO-notched FGM specimen with a material variation in the x-direction under mode I, the outer boundary can be determined by a numerical approach using the following equations. For more details please see Ref. [53].

(8)x=a-r0+(RC(x)+r0)cos(θ)y=(RC(x)+r0)sin(θ)RC(x)=(1+v(x))(5-8v(x))4πKIc(x)σut(x)2

where x and y are the coordinates of a point on the outer boundary, θ is the corresponding angle to that point (see Fig. 6), a is notch depth, $R_c(x)$ is the critical length as a function of x-coordinate, and r_0 can be evaluated by Eq. (7).

4. The SED criterion in fracture assessment of VO-notched W-Cu FGM specimens

As stated before, according to SED criterion, fracture occurs when the averaged strain energy density over a well-defined control volume reaches its critical value W_c.

In functionally graded materials, W_c is not constant all over the specimen. The initiation of fracture depends on the value of W_c corresponding to the notch tip.

In order to obtain the averaged value of SED over the control volume, some finite element analyses were carried out by using ABAQUS software version 6.11. Various

geometries have been considered in numerical analyses in order to assess the effect of notch geometries on fracture load. For each geometry, a model was created and the boundary of control volume which was obtained by a numerical approach was accurately defined. All the finite element analyses were carried out under plane strain conditions and linear elastic hypothesis. Eight-node elements were used in analyses. The contour lines of the maximum principal stress and strain energy density are shown in Fig. 7a–d. Table 4, Table 5, Table 6present the values of W_c, the averaged strain energy density SED, and theoretical fracture load F_{th} for different values of notch tip radius and notch depth. Table 4, Table 5, Table 6 are related to notch opening angles 60, 90, and 120°, respectively.

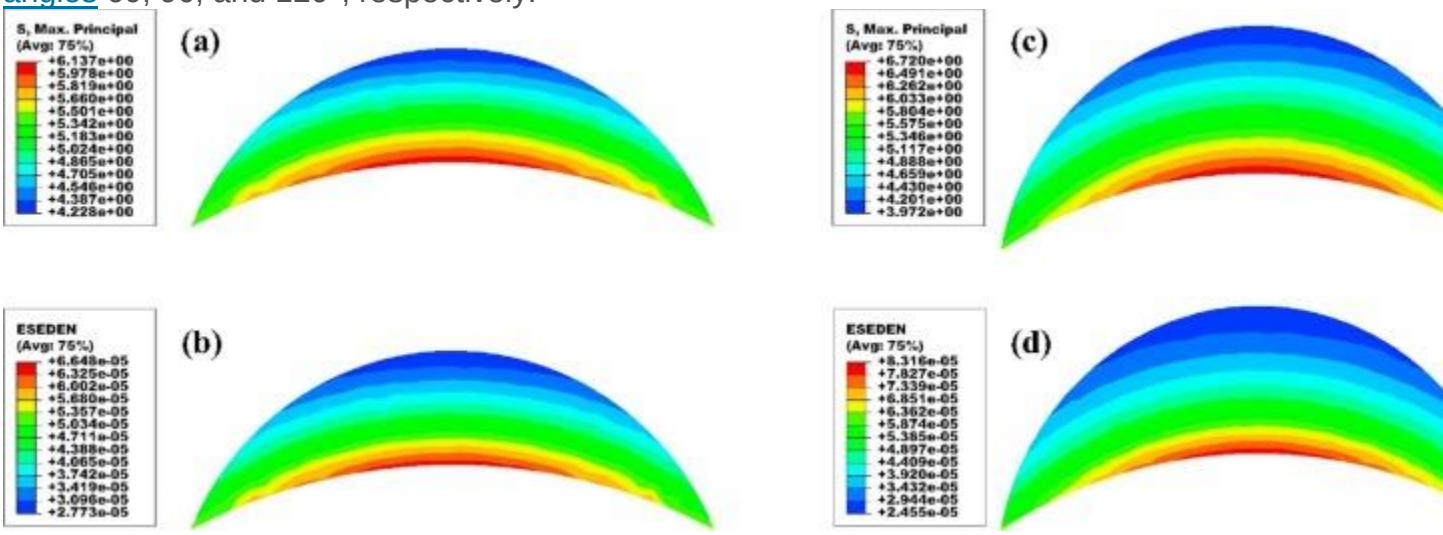

1. Download high-res image (181KB)
2. Download full-size image

Fig. 7. Contour lines of the maximum principal stress (stresses are in MPa) and the SED in the case ρ = 0.2 mm and 2α = 90° with a = 1.30 mm (a and b) and a = 1.45 mm (c and d).

Table 4. Theoretical values of SED and fracture load (F_{th}) for notch opening angle equal to 60° (The SED in this table has been evaluated applying F = 1 N in finite element models).

Model No.	ρ (mm)	a (mm)	2α (°)	W_c (MJ/m³)	SED (J/m³)	F_{th} (N)
1	0.05	1	60	0.348	59.294	76.635
2	0.1	1	60		47.492	85.629
3	0.15	1	60		38.293	95.361
4	0.2	1	60		32.734	103.141
5	0.25	1	60		28.399	110.733
6	0.3	1	60		25.589	116.655

Model No.	ρ (mm)	a (mm)	2α (°)	W_c (MJ/m^3)	SED (J/m^3)	F_{th} (N)
7	0.35	1	60		23.325	122.186
8	0.4	1	60		21.446	127.425
9	0.45	1	60		19.913	132.240
10	0.05	1.05	60	0.349	61.140	75.599
11	0.1	1.1	60	0.350	53.596	80.797
12	0.05	1.15	60	0.350	67.020	72.245
13	0.1	1.15	60		55.995	79.037
14	0.15	1.15	60		46.355	86.868
15	0.2	1.15	60		39.123	94.557
16	0.25	1.15	60		34.178	101.165
17	0.3	1.15	60		30.579	106.953
18	0.35	1.15	60		27.965	111.840
19	0.4	1.15	60		25.740	116.576
20	0.45	1.15	60		23.930	120.902
21	0.5	1.15	60		22.444	124.840
22	0.55	1.15	60		21.120	128.696
23	0.2	1.2	60	0.349	41.104	92.180
24	0.25	1.25	60	0.348	37.864	95.916
25	0.05	1.3	60	0.347	68.319	71.278
26	0.1	1.3	60		60.536	75.721
27	0.15	1.3	60		51.356	82.211
28	0.2	1.3	60		44.600	88.218
29	0.25	1.3	60		39.466	93.781
30	0.3	1.3	60		35.638	98.689
31	0.35	1.3	60		32.542	103.276
32	0.4	1.3	60		30.136	107.320
33	0.45	1.3	60		28.068	111.203
34	0.5	1.3	60		26.318	114.842
35	0.55	1.3	60		24.896	118.077
36	0.6	1.3	60		23.747	120.899
37	0.35	1.35	60	0.346	33.875	100.998
38	0.4	1.4	60	0.344	32.268	103.206
39	0.05	1.45	60	0.342	57.808	76.873

Model No.	ρ (mm)	a (mm)	2α (°)	W_c (MJ/m^3)	SED (J/m^3)	F_{th} (N)
40	0.1	1.45	60		56.033	78.081
41	0.15	1.45	60		50.600	82.166
42	0.2	1.45	60		45.662	86.495
43	0.25	1.45	60		41.399	90.839
44	0.3	1.45	60		38.062	94.738
45	0.35	1.45	60		35.233	98.468
46	0.4	1.45	60		32.986	101.766
47	0.45	1.45	60		31.025	104.933
48	0.5	1.45	60		29.308	107.964
49	0.55	1.45	60		28.015	110.427
50	0.6	1.45	60		26.743	113.021
51	0.5	1.5	60	0.339	29.689	106.902
52	0.55	1.55	60	0.337	28.185	109.302
53	0.05	1.6	60	0.334	36.994	95.011
54	0.1	1.6	60		38.700	92.893
55	0.15	1.6	60		37.465	94.412
56	0.2	1.6	60		35.897	96.452
57	0.25	1.6	60		34.134	98.912
58	0.3	1.6	60		32.460	101.430
59	0.35	1.6	60		31.028	103.744
60	0.4	1.6	60		29.742	105.963
61	0.45	1.6	60		28.583	108.089
62	0.5	1.6	60		27.585	110.029
63	0.55	1.6	60		26.685	111.869
64	0.6	1.6	60		25.832	113.700

Table 5. Theoretical values of SED and fracture load (F_{th}) for notch opening angle equal to 90° (The SED in this table has been evaluated applying F = 1 N in finite element models).

Model No.	ρ (mm)	a (mm)	2α (°)	W_c (MJ/m^3)	SED (J/m^3)	F_{th} (N)
1	0.05	1	90	0.348	57.966	77.508
2	0.1	1	90		48.411	84.813
3	0.15	1	90		39.235	94.210
4	0.2	1	90		33.290	102.276

Model No.	ρ (mm)	a (mm)	2α (°)	W_c (MJ/m^3)	SED (J/m^3)	F_{th} (N)
5	0.25	1	90		29.317	108.986
6	0.3	1	90		25.928	115.890
7	0.35	1	90		23.472	121.804
8	0.4	1	90		21.570	127.058
9	0.45	1	90		19.908	132.255
10	0.05	1.05	90	0.349	61.361	75.443
11	0.1	1.1	90	0.350	54.126	80.401
12	0.05	1.15	90	0.350	62.465	74.833
13	0.1	1.15	90		56.803	78.473
14	0.15	1.15	90		46.944	86.321
15	0.2	1.15	90		39.938	93.587
16	0.25	1.15	90		34.755	100.323
17	0.3	1.15	90		31.114	106.030
18	0.35	1.15	90		28.242	111.291
19	0.4	1.15	90		25.990	116.013
20	0.45	1.15	90		24.096	120.485
21	0.5	1.15	90		22.642	124.294
22	0.55	1.15	90		21.245	128.316
23	0.2	1.2	90	0.349	42.296	90.871
24	0.25	1.25	90	0.348	38.885	94.649
25	0.05	1.3	90	0.347	61.281	75.260
26	0.1	1.3	90		60.506	75.740
27	0.15	1.3	90		52.443	81.354
28	0.2	1.3	90		44.938	87.886
29	0.25	1.3	90		40.272	92.837
30	0.3	1.3	90		36.195	97.927
31	0.35	1.3	90		32.900	102.714
32	0.4	1.3	90		30.418	106.822
33	0.45	1.3	90		28.297	110.753
34	0.5	1.3	90		26.638	114.149
35	0.55	1.3	90		25.223	117.309
36	0.6	1.3	90		23.891	120.533
37	0.35	1.35	90	0.346	34.204	100.511

Model No.	ρ (mm)	a (mm)	2α (°)	W_c (MJ/m³)	SED (J/m³)	F_{th} (N)
38	0.4	1.4	90	0.344	32.600	102.681
39	0.05	1.45	90	0.342	57.331	77.192
40	0.1	1.45	90		56.567	77.712
41	0.15	1.45	90		51.287	81.614
42	0.2	1.45	90		46.090	86.092
43	0.25	1.45	90		41.954	90.237
44	0.3	1.45	90		38.573	94.108
45	0.35	1.45	90		35.764	97.734
46	0.4	1.45	90		33.341	101.223
47	0.45	1.45	90		31.319	104.440
48	0.5	1.45	90		29.636	107.365
49	0.55	1.45	90		28.243	109.980
50	0.6	1.45	90		26.944	112.600
51	0.5	1.5	90	0.339	30.012	106.324
52	0.55	1.55	90	0.337	28.432	108.827
53	0.05	1.6	90	0.334	36.375	95.816
54	0.1	1.6	90		38.618	92.992
55	0.15	1.6	90		37.787	94.010
56	0.2	1.6	90		36.278	95.944
57	0.25	1.6	90		34.350	98.600
58	0.3	1.6	90		32.774	100.942
59	0.35	1.6	90		31.285	103.317
60	0.4	1.6	90		29.979	105.544
61	0.45	1.6	90		28.848	107.593
62	0.5	1.6	90		27.786	109.630
63	0.55	1.6	90		26.893	111.434
64	0.6	1.6	90		26.037	113.251

Table 6. Theoretical values of SED and fracture load (F_{th}) for notch opening angle equal to 120° (The SED in this table has been evaluated applying F = 1 N in finite element models).

Model No.	ρ (mm)	a (mm)	2α (°)	W_c (MJ/m³)	SED (J/m³)	F_{th} (N)
1	0.05	1	120	0.348	52.202	81.674
2	0.1	1	120		46.416	86.616

Model No.	ρ (mm)	a (mm)	2α (°)	W_c (MJ/m^3)	SED (J/m^3)	F_{th} (N)
3	0.15	1	120		38.998	94.495
4	0.2	1	120		33.839	101.443
5	0.25	1	120		29.632	108.405
6	0.3	1	120		26.422	114.802
7	0.35	1	120		23.737	121.120
8	0.4	1	120		21.791	126.413
9	0.45	1	120		19.985	132.002
10	0.05	1.05	120	0.349	55.140	79.606
11	0.1	1.1	120	0.350	51.455	82.461
12	0.05	1.15	120	0.350	59.249	76.837
13	0.1	1.15	120		54.446	80.154
14	0.15	1.15	120		46.218	86.996
15	0.2	1.15	120		39.834	93.709
16	0.25	1.15	120		35.458	99.323
17	0.3	1.15	120		31.615	105.187
18	0.35	1.15	120		28.592	110.607
19	0.4	1.15	120		26.126	115.709
20	0.45	1.15	120		24.179	120.278
21	0.5	1.15	120		22.697	124.142
22	0.55	1.15	120		21.447	127.711
23	0.2	1.2	120	0.349	41.562	91.670
24	0.25	1.25	120	0.348	38.963	94.554
25	0.05	1.3	120	0.347	60.523	75.730
26	0.1	1.3	120		58.348	77.128
27	0.15	1.3	120		51.566	82.043
28	0.2	1.3	120		45.215	87.616
29	0.25	1.3	120		40.067	93.074
30	0.3	1.3	120		36.426	97.616
31	0.35	1.3	120		33.201	102.246
32	0.4	1.3	120		30.710	106.313
33	0.45	1.3	120		28.676	110.018
34	0.5	1.3	120		26.918	113.555
35	0.55	1.3	120		25.401	116.896

Model No.	ρ (mm)	a (mm)	2α (°)	W_c (MJ/m^3)	SED (J/m^3)	F_{th} (N)
36	0.6	1.3	120		24.097	120.018
37	0.35	1.35	120	0.346	34.550	100.006
38	0.4	1.4	120	0.344	32.942	102.146
39	0.05	1.45	120	0.342	50.904	81.921
40	0.1	1.45	120		53.577	79.851
41	0.15	1.45	120		50.103	82.573
42	0.2	1.45	120		45.874	86.295
43	0.25	1.45	120		42.028	90.157
44	0.3	1.45	120		38.749	93.894
45	0.35	1.45	120		35.992	97.424
46	0.4	1.45	120		33.689	100.700
47	0.45	1.45	120		31.751	103.726
48	0.5	1.45	120		30.033	106.652
49	0.55	1.45	120		28.594	109.302
50	0.6	1.45	120		27.355	111.752
51	0.5	1.5	120	0.339	30.309	105.802
52	0.55	1.55	120	0.337	28.711	108.296
53	0.05	1.6	120	0.334	32.606	101.203
54	0.1	1.6	120		36.345	95.856
55	0.15	1.6	120		36.662	95.440
56	0.2	1.6	120		35.644	96.794
57	0.25	1.6	120		34.254	98.739
58	0.3	1.6	120		32.869	100.797
59	0.35	1.6	120		31.477	103.002
60	0.4	1.6	120		30.222	105.119
61	0.45	1.6	120		29.053	107.212
62	0.5	1.6	120		27.994	109.221
63	0.55	1.6	120		27.100	111.009
64	0.6	1.6	120		26.206	112.886

5. Comparison between experimental and theoretical fracture loads

A comparison between average values of experimental fracture loads (F_{EXP}) and theoretical ones (F_{th}) calculated by SED criterion has been made in Table 7. A good agreement can be clearly seen from this table.

Table 7. Comparison between experimental (F_{EXP}) and theoretical (F_{th}) fracture loads.

ρ (mm)	b (mm)	2α (°)	F_{EXP} (N)	F_{th} (N)	F_{EXP}/F_{th}
0.3	1	60	96.1	98.689	0.973
0.4	1	60	105.1	103.206	1.018
0.6	1	60	121.4	113.700	1.068
0.3	1	90	100.2	97.927	1.024
0.4	1	90	107.3	102.681	1.045
0.6	1	90	119.2	113.251	1.052
0.3	1	120	88.4	97.616	0.906
0.4	1	120	107.3	102.146	1.050
0.6	1	120	116.2	112.886	1.029

In addition in Fig. 8a–c, a comparison between experimental fracture loads and theoretical predictions was made for notch opening angles 60, 90, and 120°. The plots are given for a constant center of curvature's depth (b = 1 mm). In other words, in these plots, the notch depth (a) varies by changing the notch tip radius. The agreement between experimental and theoretical fracture loads is quite satisfactory. The trend of experimental and theoretical fracture loads are in a good agreement.

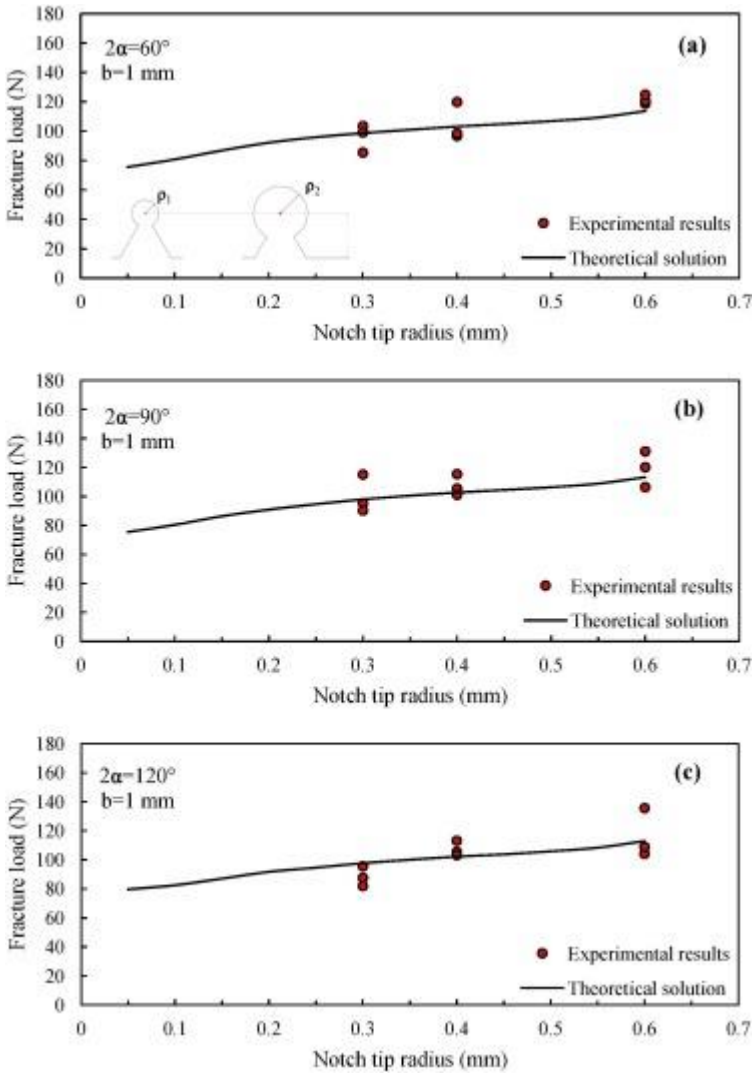

1. Download high-res image (276KB)
2. Download full-size image

Fig. 8. Comparison between experimental and theoretical fracture loads for b = 1 mm and 2α = 60° (a), 2α = 90° (b), and 2α = 120°.

A synthesis in terms of the square root value of the SED averaged over the control volume, normalized with respect to the critical energy of the material, as a function of the notch tip radius is shown in Fig. 9. The normalized scatter band is plotted based on new data for SENB VO-notched W-Cu FGM specimens under mode I loading. At first sight, it can be noted that the scatter is almost independent of the notch tip radius. Almost all values fall inside a band ranges from 0.8 to 1.2. The synthesis confirms that SED is applicable to predict the fracture load of VO-notched specimens made of functionally graded materials.

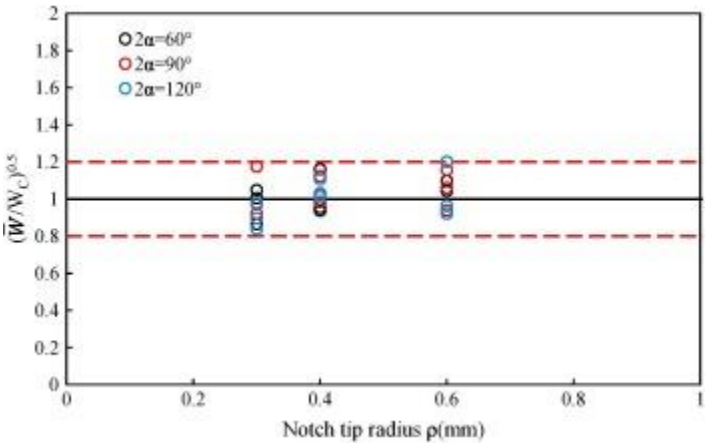

1. Download high-res image (100KB)
2. Download full-size image

Fig. 9. Scatter band summarizing new data for VO-notched W-Cu FGM under mode I.

6. Effect of notch geometry on fracture load

In this section, the effect of notch geometry such as notch tip radius (ρ) and notch depth (a) on fracture load have been assessed. All the figures are plotted based on theoretical results derived in Section 4. The variation of fracture load with respect to the notch tip radius is shown in Fig. 10a–e. Each curve is plotted keeping constant the notch depth (a) and the notch opening angle. In Fig. 10a–e, the fracture loads of three notch opening angles 60, 90, and 120° have been compared. At first sight, it is obvious that fracture load is almost independent of the notch opening angle especially for notch tip radii greater than 0.1 mm. The greater the notch tip radius, the less dependence of the fracture load on notch opening angle. For a constant notch tip radius less than 0.1 mm and a constant notch depth, as expected, the fracture load increases with increasing the notch opening angle. It can clearly be observed that the effect of notch tip radius on fracture load has been faded by increasing the notch depth. It should be noted that in order to make sure that the trends are accurate and they can describe the material behavior, some additional experimental data are required.

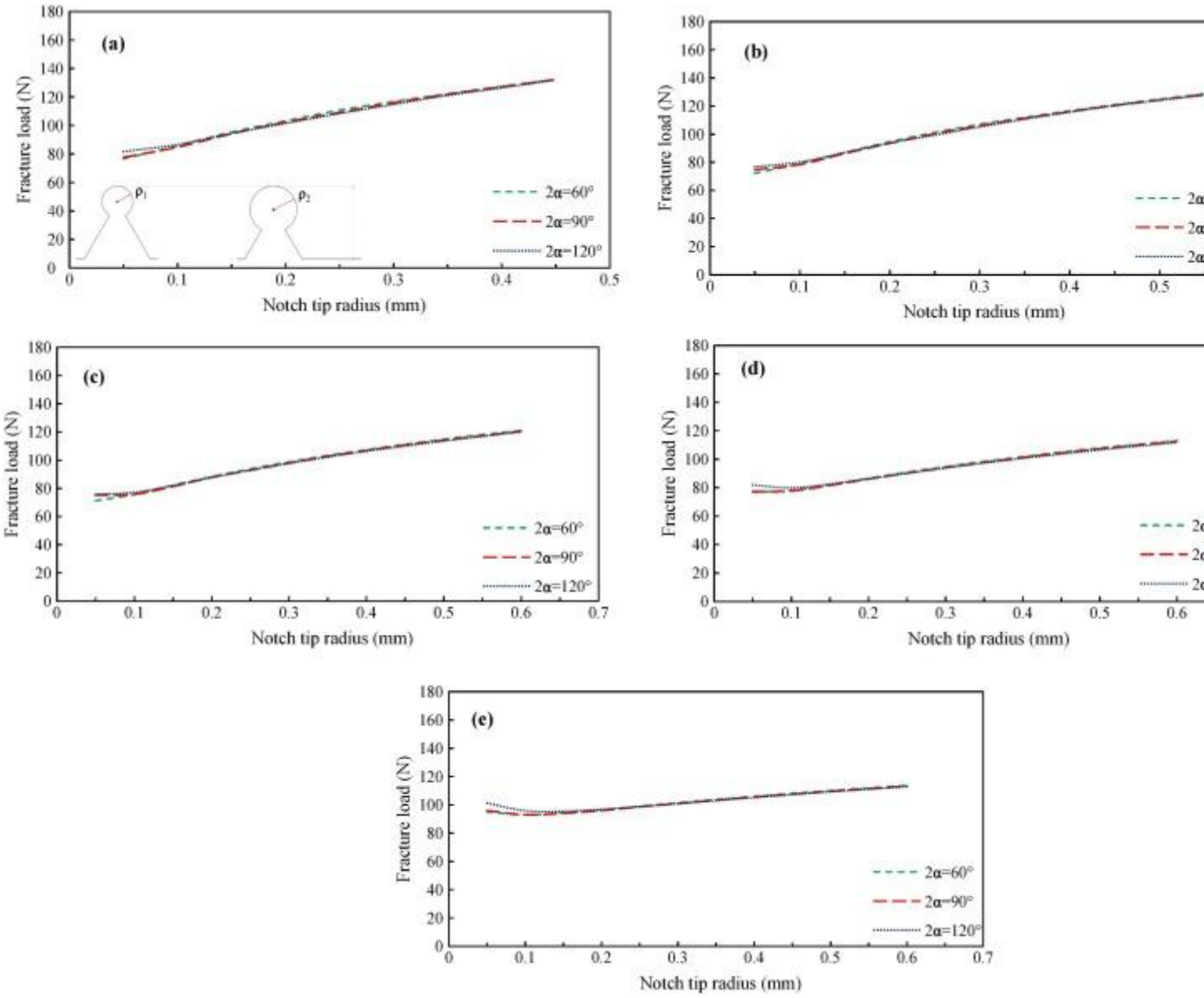

1. Download high-res image (459KB)
2. Download full-size image

Fig. 10. The variation of fracture load with respect to the notch tip radius for notch depth *a* = 1 mm (a), *a* = 1.15 mm (b), *a* = 1.30 mm (c), *a* = 1.45 mm (d), and *a* = 1.60 mm (e).

The effect of notch depth (*a*) on the fracture load has been assessed in Fig 11a–c. Each curve is plotted keeping constant the notch root radius and the notch opening angle. In a constant notch tip radius and notch opening angle, it can be observed that with increasing the notch depth, the fracture load shows a downward trend to a minimum value and then the trend becomes upward. The initial decrease can be justified with respect to stress concentration. However, the following increase in fracture load is

mainly because the size of control volume expands remarkably since by increasing the notch depths, as a result of the material gradient, the notch tip is placed in a material with a greater fracture toughness and a smaller ultimate tensile stress. It should be noted that the maximum variation of W_c with respect to the notch tip is 5% (Table 4, Table 5, Table 6) and this value does not have a very considerable effect on trends of Fig. 11.

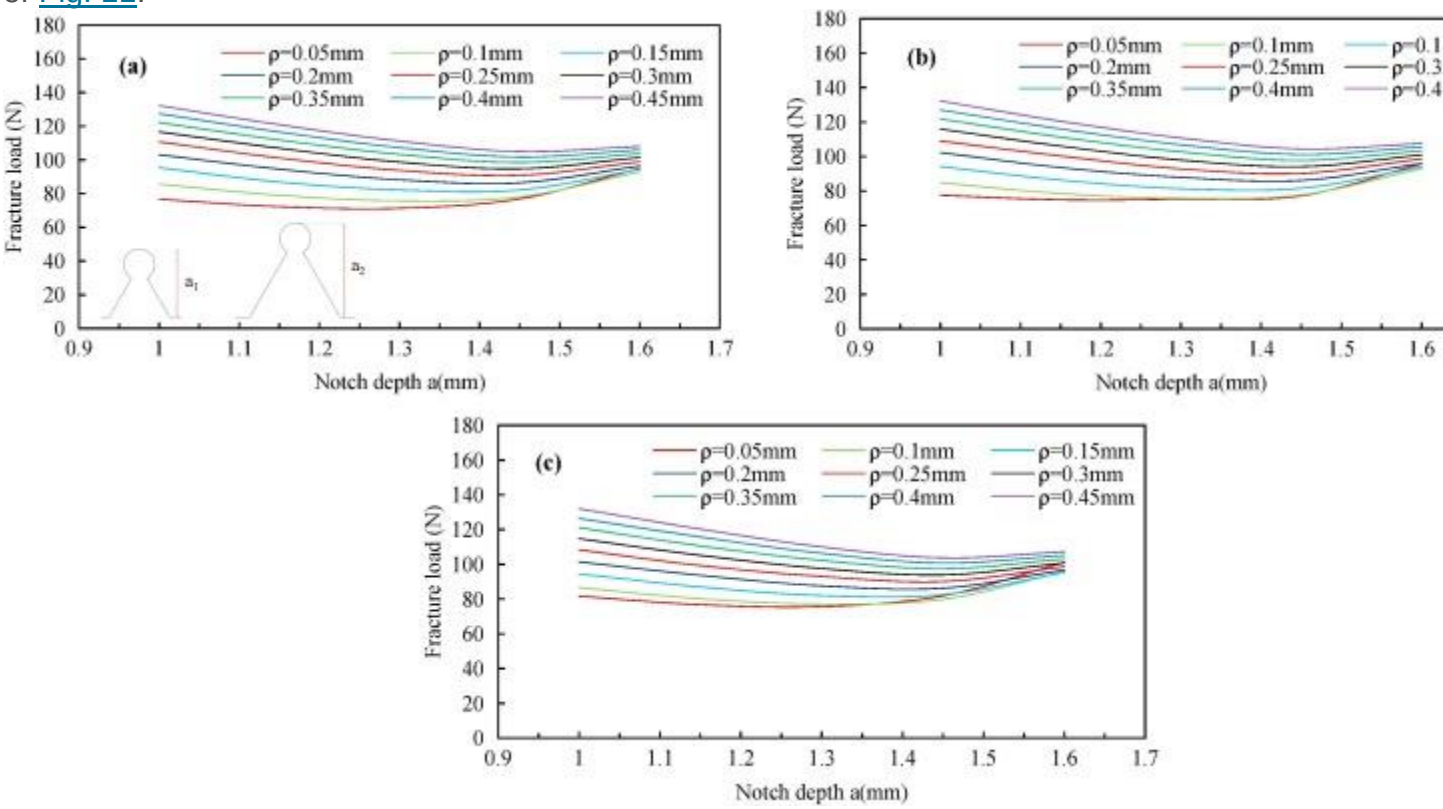

1. Download high-res image (499KB)
2. Download full-size image

Fig. 11. The variation of fracture load with respect to the notch depth for notch opening angle $2\alpha = 60°$ (a), $2\alpha = 90°$ (b), and $2\alpha = 120°$ (c).

7. Conclusion

In the present research, the averaged strain energy density criterion was employed to predict the critical load of VO-notched specimens made of W-Cu FGM under mode I loading. The main findings of this research have been summarized as follows:

1.

A six-layered W-Cu FGM was successfully fabricated by powder metallurgy technique. A new set of experimental data on fracture of VO-notched W-Cu FGM was presented in this work.

2.
The approach based on the SED was successfully extended to the FGMs with variant elasticity modulus and Poisson's ratio. The outer boundary of the control volume was determined numerically.

3.
The effect of notch geometry (notch tip radius, notch depth, and notch opening angle) on the critical fracture load was elaborated.

4.
The average discrepancy between experimental and theoretical fracture loads was found to be 4.5%.

5.
The shape and size of control volume were appropriate for W-Cu FGM.